Theoretical analysis of three-dimensional polaritonic photonic crystals

G. Gantzounis and N. Stefanou
University of Athens, Section of Solid State Physics, Panepistimioupolis, GR-157 84 Athens, Greece
(Received 10 May 2005; revised manuscript received 7 June 2005; published 2 August 2005)

The optical properties of three-dimensional photonic crystals consisting of polaritonic spheres in a dielectric host medium are studied by means of accurate numerical calculations using the on-shell layer-multiple-scattering method. The transmission characteristics of finite slabs of these materials are related to the complex band structure of the corresponding infinite crystals and the effect of dissipative losses is examined.

DOI: 10.1103/PhysRevB.72.075107 PACS number(s): 42.70.Qs, 42.25.Bs, 71.36.+c, 71.15.−m

I. INTRODUCTION

Photonic crystals, composite materials whose dielectric function or/and magnetic permeability varies periodically in space on a macroscopic length scale, provide impressive opportunities for tailoring the light-matter interaction.[1,2] In recent years, considerable effort has been devoted to the investigation of the so-called polaritonic photonic crystals.[3–14] These are made of heteropolar semiconducting or insulating materials which have a strongly dispersive dielectric function in the infrared region, and exhibit new exciting physical phenomena such as flux expulsion and node switching,[9,10] negative effective magnetic permeability over selected regions of frequency,[13,14] etc. However, most of the above studies refer to two-dimensional polaritonic photonic crystals. The purpose of the present paper is to report a thorough investigation of three-dimensional crystals of polaritonic spheres in a homogeneous dielectric host medium, by means of first-principles calculations using the on-shell layer-multiple-scattering method.[15–17] This method is ideally suited for photonic crystals with absorptive and/or strongly dispersive constituents such as polaritonic materials. In addition to the complex frequency band structure of the (infinite) photonic crystal associated with a given crystallographic plane, the method allows one to calculate, also, the transmission, reflection, and absorbtion coefficients of an electromagnetic (EM) wave incident at a given angle on a finite slab of the crystal and, therefore, it can describe an actual transmission experiment.

The band structure of the photonic crystals under consideration is characterized by flat, almost dispersionless bands which originate from the resonance modes of the individual spheres. We show how hybridization between such narrow bands and a wide band corresponding to propagation in an effective medium leads to the appearance of frequency gaps. We find that an absolute gap can be formed by this mechanism and its width increases with the fractional volume occupied by the spheres. The symmetry and optical activity of the different bands are analyzed in conjunction with relevant transmission spectra, and the effect of dissipative losses in the polaritonic material is examined. Our analysis elucidates the complex optical response of these systems and provides a transparent picture of the underlying physical processes.

II. EIGENMODES OF A SINGLE POLARITONIC SPHERE

In usual heteropolar semiconductors or insulators, the photon-phonon interaction leads to a strongly dispersive dielectric function at infrared frequencies, which can be described by the following simple yet effective model:[18]

$$\epsilon_s(\omega) = \epsilon_\infty + \frac{\epsilon_0 - \epsilon_\infty}{1 - (\omega/\omega_T)(\omega/\omega_T + i\Gamma/\omega_T)}, \qquad (1)$$

where ϵ_0 and ϵ_∞ are the static and optical dielectric constants, respectively, and ω_T is the long-wavelength transverse optical phonon frequency. As can be seen from Fig. 1(a), $\epsilon_s(\omega)$ has a resonance at ω_T. The width of this resonance is characterized by Γ, a damping factor accounting for absorption which is intimately connected with a resonance. In the absence of absorption ($\Gamma=0$), the above dielectric function has an asymptote at $\omega=\omega_T$ and vanishes at $\omega_L=\omega_T\sqrt{\epsilon_0/\epsilon_\infty}$, the long-wavelength longitudinal optical phonon frequency. In the frequency region from ω_T to ω_L the dielectric function is negative, thus not allowing EM waves to propagate in the material, and this region is referred to as polariton gap because the quasiparticle which results from the photon-phonon coupling is called polariton. Clearly, the power of

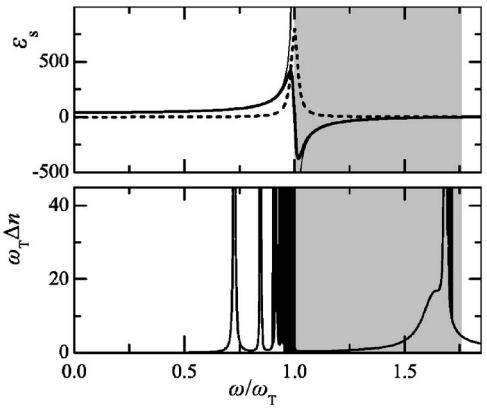

FIG. 1. (a) The real (thick solid line) and imaginary (dashed line) parts of the polaritonic model dielectric function of $LiTaO_3$ ($\epsilon_0=41.4, \epsilon_\infty=13.4, \Gamma=0.035\omega_T$). The (real) dielectric function in the absence of absorption ($\Gamma=0$) is shown by the thin solid line. (b) The change in the density of states Δn induced by a nonabsorbing $LiTaO_3$ sphere of radius $S=0.5c/\omega_T$ in air. The shaded regions indicate the frequency interval of the polariton gap.

polaritonic materials lies in the opportunity to study the large-ϵ and negative-ϵ regimes using the same physical structure by merely choosing the frequency of light below ω_T or inside the polariton gap between ω_T and ω_L. In this paper we shall consider spheres made of a polaritonic material and we shall use ω_T as the unit of frequency. For the purpose of numerical computation we take $\epsilon_0=41.4$, $\epsilon_\infty=13.4$, and $\Gamma=0.035\omega_T$, which correspond to $LiTaO_3$.[19]

We assume, to begin with, a single $LiTaO_3$ sphere of radius S in air and we neglect losses for now. This sphere supports states for which the EM field is mostly localized at the sphere and leaks to some minor degree in the host region. These states are referred to as virtual bound states. They are obtained at the poles of the elements of the corresponding scattering matrix $\mathbf{T}$

$$T_{El}=\left[\frac{j_l(x_s)[xj_l(x)]'\epsilon_s-j_l(x)[x_sj_l(x_s)]'}{h_l^+(x)[x_sj_l(x_s)]'-j_l(x_s)[xh_l^+(x)]'\epsilon_s}\right]_{x=\omega S/c;x_s=\sqrt{\epsilon_s}x},$$

$$T_{Hl}=\left[\frac{j_l(x_s)[xj_l(x)]'-j_l(x)[x_sj_l(x_s)]'}{h_l^+(x)[x_sj_l(x_s)]'-j_l(x_s)[xh_l^+(x)]'}\right]_{x=\omega S/c;x_s=\sqrt{\epsilon_s}x}, \tag{2}$$

c being the velocity of light in vacuum and $j_l(h_l^+)$ the spherical Bessel (Hankel) functions, in the lower complex-frequency half-plane close to the real axis at $z_l=\omega_l-i\gamma_l$;[20] ω_l is the eigenfrequency while γ_l $(0<\gamma_l\ll\omega_l)$ denotes the inverse of the lifetime of the respective 2^l-pole virtual bound state. It can be shown that such poles of both types, electric (pole of T_{El}) and magnetic (pole of T_{Hl}), exist below ω_T where the dielectric function is strongly positive. An asymptotic analysis, in the limit $\omega\to\omega_T$, leads to the following approximate expression for the eigenfrequencies of these modes

$$\frac{\omega_{nl}}{\omega_T}\approx 1-\frac{2(\epsilon_0-\epsilon_\infty)(\omega_TS/c)^2}{\pi^2}\frac{1}{(n+l)^2},\ n=1,2,3,\ldots, \tag{3}$$

for each value of l $(l=1,2,3,\ldots)$. For odd and even values of n we obtain the solutions of magnetic and electric type, respectively. It is obvious that there is an infinite number of such solutions which are accumulated at ω_T. Of course, the closer we get to ω_T the better the above approximation becomes. Virtual bound states, but only of electric type, exist also inside the polariton gap. These are similar to the surface-plasmon resonance states of a metallic sphere and, for a small sphere, they are obtained at

$$\frac{\omega_l}{\omega_T}\approx\sqrt{\frac{l\epsilon_0+l+1}{l\epsilon_\infty+l+1}}, \tag{4}$$

for each value of l. It is easy to see that the above states, for large values of l, are accumulated at $\omega_T\sqrt{(\epsilon_0+1)/(\epsilon_\infty+1)}$.

In Fig. 1(b) we show the change in the density of states Δn induced by a single non-absorbing $LiTaO_3$ sphere in air. This is calculated from[20]

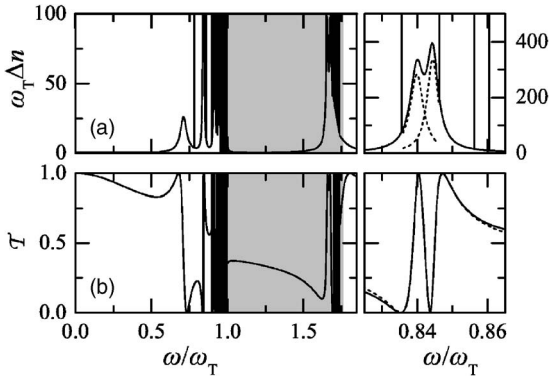

FIG. 2. A square array, with lattice constant $a=1.1c/\omega_T$, of nonabsorbing $LiTaO_3$ spheres, with radius $S=0.5c/\omega_T$, in air. Change in the density of states of the system with respect to air for $\mathbf{k}_\parallel=\mathbf{0}$ (a), and transmittance at normal incidence (b). The shaded regions indicate the frequency interval of the polariton gap. The region about the first dipole electric and quadrupole magnetic resonances of the single sphere below the polariton gap are shown with a higher resolution in the right panel.

$$\Delta n(\omega)=\frac{d}{d\omega}\left\{\frac{1}{\pi}\,\mathrm{Im}\ln\det[\mathbf{1}+\mathbf{T}]\right\}. \tag{5}$$

The sphere has a radius $S=0.5c/\omega_T$ which for $\omega_T=26.7$ THz [the value of the long-wavelength transverse optical phonon frequency for $LiTaO_3$ (Ref. 19)] corresponds to 5.6 μm. It can be seen that Δn is characterized by an infinite number of resonance peaks. We have confirmed that their centers are approximately given by Eqs. (3) and (4), and that they are nicely fitted by Lorentzian curves given by[20]

$$\Delta n_l(\omega)\approx\frac{2l+1}{\pi}\frac{\gamma_l}{(\omega-\omega_l)^2+\gamma_l^2}. \tag{6}$$

III. SCATTERING AND ABSORPTION BY A PLANE OF POLARITONIC SPHERES

We now consider a square array, with lattice constant $a=1.1c/\omega_T$, of nonabsorbing $LiTaO_3$ spheres with $S=0.5c/\omega_T$ in air. Because of the two-dimensional periodicity of the structure under consideration, the modes of the EM field are characterized by $\mathbf{k}_\parallel$, the component of the wave vector parallel to the plane of spheres (this is taken to be the x-y plane) reduced within the surface Brillouin zone (SBZ).

In Fig. 2(a) we show the change in the density of states induced by the plane of spheres in air, for $\mathbf{k}_\parallel=\mathbf{0}$. This is calculated from the general formula[20]

$$\Delta n(\omega,\mathbf{k}_\parallel)=\frac{\partial}{\partial\omega}\left\{\frac{1}{2\pi}\,\mathrm{Im}\ln\det\mathbf{S}\right\}, \tag{7}$$

where $\mathbf{S}$ is obtained directly from the transmission and reflection matrices of the plane of spheres, for the given ω and $\mathbf{k}_\parallel$.[20] As can be seen from Fig. 2(a), the $(2l+1)$ degeneracy of the virtual bound states of the single sphere is removed because of the interaction with the other spheres of the plane. For $\mathbf{k}_\parallel=\mathbf{0}$, the states of the EM field have the symmetry of

the irreducible representations of the C_{4v} group: Δ_1, Δ_2, $\Delta_{1'}$, $\Delta_{2'}$, Δ_5.[21] The states of symmetry Δ_1, Δ_2, $\Delta_{1'}$, $\Delta_{2'}$ are nondegenerate and Δ_5 are doubly degenerate. Next to Fig. 2(a) we show in more detail the decomposition of the first dipole electric and quadrupole magnetic virtual bound states of the single sphere below the polariton gap. In agreement with a group-theory analysis,[22] the dipole electric mode gives a Δ_1 and a Δ_5 mode, while the quadrupole magnetic mode gives a Δ_2, $\Delta_{1'}$, $\Delta_{2'}$, and Δ_5 mode. We note that a plane EM wave propagating in the host region normal to the plane of spheres ($\mathbf{k}_\parallel=\mathbf{0}$) has the Δ_5 symmetry and, therefore, only modes of the plane of spheres with the same symmetry can be excited by an externally incident wave. The modes of different symmetry are inactive; they are bound states of the system and decay exponentially to zero away from the plane of spheres on either side of it. These inactive modes are delta functions in the density of states, while the optically active modes, of Δ_5 symmetry, are manifested as Lorentzian resonances in the density of states [see Fig. 2(a)]. The integral of each such Lorentzian equals 2, while its center and width determine the eigenfrequency and inverse lifetime, respectively, of the corresponding virtual bound state. For example, the first dipole electric mode of the single sphere gives a bound state of Δ_1 symmetry at $0.836\omega_T$, and a Δ_5 virtual bound state [the first Lorentzian shown by dashed lines in the right panel of Fig. 2(a)] at $\omega_1=0.840\omega_T$ with an inverse lifetime $\gamma_1=2.26\times10^{-3}\omega_T$. On the other hand, the first quadrupole magnetic mode of the single sphere gives three bound states at $0.846\omega_T$ (Δ_2), $0.856\omega_T$ ($\Delta_{1'}$), $0.861\omega_T$ ($\Delta_{2'}$), and a Δ_5 virtual bound state [the second Lorentzian shown by dashed lines in the right panel of Fig. 2(a)] at $\omega_2=0.844\omega_T$ with an inverse lifetime $\gamma_2=1.90\times10^{-3}\omega_T$.

In Fig. 2(b) we show the transmittance of the plane of spheres at normal incidence. It can be seen that the transmission spectrum is characterized by resonance structures which originate from the corresponding virtual bound states. In the frequency region about the first dipole electric and quadrupole magnetic resonances of the single sphere below the polariton gap, where there are two virtual bound states of the plane of spheres [see dashed curves in the right panel of Fig. 2(a)], the resonant transmittance is described by the following function (see Appendix):

$$\mathcal{T}=\frac{1}{2}\{1+\cos[2\delta_1(\omega)+2\delta_2(\omega)-\phi]\}, \tag{8}$$

with

$$\cos[2\delta_i(\omega)]=\frac{(\omega-\omega_i)^2-\gamma_i^2}{(\omega-\omega_i)^2+\gamma_i^2},$$

$$\sin[2\delta_i(\omega)]=\frac{-2\gamma_i(\omega-\omega_i)}{(\omega-\omega_i)^2+\gamma_i^2}, \quad i=1,2, \tag{9}$$

ω_1, ω_2 and γ_1, γ_2 being the eigenfrequencies and inverse lifetimes, respectively, of the corresponding virtual bound states. As shown by the dashed line in the right panel of Fig. 2(b), an excellent fit of the resonance structures in the transmittance is obtained by Eqs. (8) and (9) using a single adjustable parameter, ϕ (in the present case $\phi=102°$).

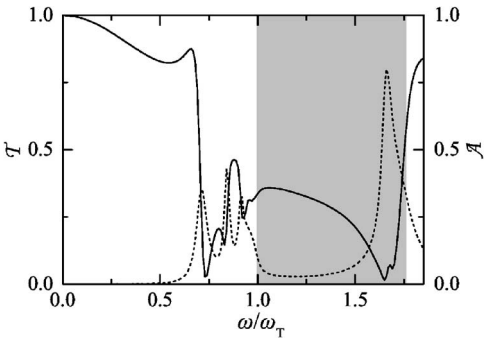

FIG. 3. Transmittance (solid line) and absorbance (dashed line) of a square array, with lattice constant $a=1.1c/\omega_T$, of absorbing $LiTaO_3$ spheres, with radius $S=0.5c/\omega_T$, in air, at normal incidence. The shaded region indicates the frequency interval of the polariton gap.

In Fig. 3 we show the transmittance and absorbance of the plane of spheres, taking into account dissipative losses in the polaritonic material ($\Gamma=0.035\omega_T$). We can see that the sharp features in the transmission spectrum, which originate from the virtual bound states with long lifetimes, are smoothed out by absorption, and essentially only the fundamental dipole and quadrupole virtual bound states of the spheres manifest themselves in the transmittance. Correspondingly, the absorption spectrum is characterized by resonance peaks in the frequency regions of the virtual bound states.

IV. PHOTONIC CRYSTALS OF POLARITONIC SPHERES

We now consider a simple cubic (sc) crystal of nonabsorbing $LiTaO_3$ spheres in air, where the fractional volume occupied by the spheres is $f=39.3\%$, and we view the crystal as a sequence of (001) planes of spheres. Figure 4(a) shows the photonic band structure normal to the (001) surface. The symmetry of the bands along this direction $(\Delta_1,\Delta_2,\Delta_{1'},\Delta_{2'},\Delta_5)$ is that of the C_{4v} group.[21] The bands Δ_1, Δ_2, $\Delta_{1'}$, $\Delta_{2'}$ are nondegenerate and Δ_5 is doubly degenerate. We note that the (001) surface of the crystal under consideration is a plane of mirror symmetry and, therefore, the frequency bands appear in pairs $k_z(\omega,\mathbf{k}_\parallel)$ and $-k_z(\omega,\mathbf{k}_\parallel)$; for this reason, in Fig. 4(a), we show the bands only for positive k_z.

Away from the region of the polariton gap we obtain a linear dispersion curve, of Δ_5 symmetry, as expected for propagation in a homogeneous effective medium with a frequency-independent dielectric constant[23] $\bar{\epsilon}_{0(\infty)}=[\epsilon_{0(\infty)}(1+2f)+2(1-f)]/[\epsilon_{0(\infty)}(1-f)+(2+f)]$ below (above) the polariton gap. About the region of this gap the frequency band structure is dominated by flat resonance bands which originate from the virtual bound states of the $LiTaO_3$ spheres. The Δ_5 component of these bands hybridizes with the extended Δ_5 band that would be in the dielectric effective medium to produce the Δ_5 bands in the photonic crystal shown in Fig. 4(a). It can be seen that frequency gaps open up due to hybridization between the extended band and flat bands with the same symmetry. The hybridization is stronger for the fundamental dipole resonance bands, because of the larger

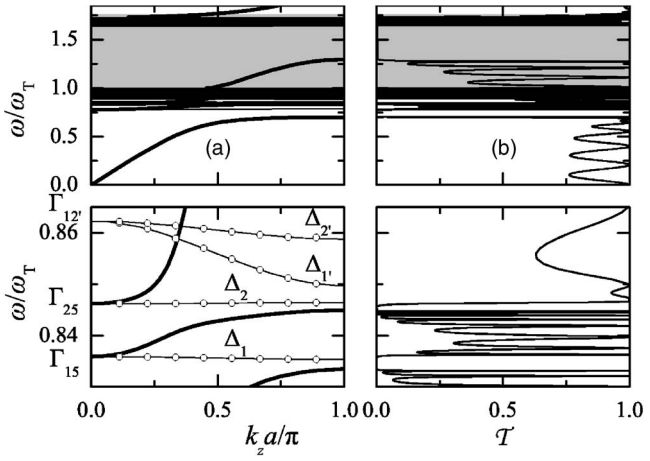

FIG. 4. (a) The photonic band structure of a sc photonic crystal of nonabsorbing $LiTaO_3$ spheres ($S=0.5c/\omega_T$) in air, with $f=39.3\%$, along the [001] direction. (b) Transmittance at normal incidence of a slab of $N_L=8$ (001) planes of spheres of the above crystal. The shaded regions indicate the frequency interval of the polariton gap. The region about the first dipole electric and quadrupole magnetic resonances of the single sphere below the polariton gap are shown with a higher resolution in the lower panel. The thick (thin) lines refer to doubly degenerate (nondegenerate) bands.

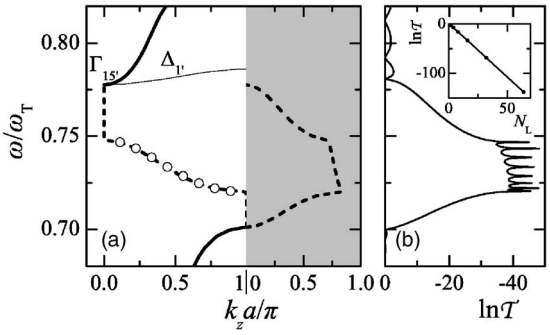

FIG. 5. A detail view of diagrams (a) and (b) of Fig. 4 over a limited frequency region about the first dipole magnetic resonance of the single sphere. In the band-structure diagram (a), over the frequency gap, we show by broken lines the real-frequency lines with the smallest imaginary part. The imaginary part is shown in the shaded region. In the inset of the transmittance diagram (b) we show the transmittance at a given frequency $\omega=0.71\omega_T$ within the gap as a function of the thickness of the slab (filled circles). The straight line has a slope equal to $-2a\,\mathrm{Im}[k_z]$, where $\mathrm{Im}[k_z]$ is the smallest imaginary part of $k_z(0.71\omega_T,\mathbf{k}_\parallel=\mathbf{0})$.

spatial extent of the associated wave function, and the corresponding gaps are wider. It should be noted that the gaps considered in this paper are unrelated to Bragg scattering and thus can be described, to some extent, by using effective-medium theory: A Mie dipole resonance of electric or magnetic type may induce a negative effective dielectric function or magnetic permeability, respectively, over a corresponding region of frequency.[23] However, the effective-medium theories are valid in the long-wavelength limit and rely on the dipole approximation. They cannot describe the detailed actual photonic band structure and are unable to account for the anisotropic properties of the crystal.

The nondegenerate bands in Fig. 4(a) arise from an apparently weak interaction between the corresponding bound states of the EM field, localized about consecutive (001) planes of spheres [see Fig. 2(a)]. In order to demonstrate the above, we looked for the eigenmodes of the EM field, for $\mathbf{k}_\parallel=\mathbf{0}$, in a slab of $N_L=8$ planes of spheres, in the manner described in Ref. 24. Over the frequency range of each of these bands we obtain eight eigenfrequencies which, plotted against values of the reduced wave number $k_z=\kappa\pi/(N_L+1)a$, $\kappa=1,2,\ldots,N_L$, ($N_L=8$), reproduce the corresponding dispersion curves of the infinite crystal, as shown by the open circles in the lower panel of Fig. 4(a). According to the discussion in the previous section, the nondegenerate bands along the [001] direction of the crystal cannot be excited by an externally incident wave because they do not have the proper symmetry. However, these bands survive for $\mathbf{k}_\parallel\neq\mathbf{0}$ (at least in the neighborhood of $\mathbf{k}_\parallel=\mathbf{0}$), where they couple with an incident wave of the same $\mathbf{k}_\parallel$ leading to measurable transmittance.

We note that the total number of bands shown in Fig. 4(a) equals the number expected from the degeneracy of the resonances of the individual spheres in hybridization with a "would be" extended effective-medium band. For example, as can be seen in the lower panel of Fig. 4(a), the dipole electric virtual bound states of the individual spheres give a threefold degenerate mode (of Γ_{15} symmetry) at $\mathbf{k}=\mathbf{0}$ which is separated into a Δ_1 and a Δ_5 band along the [001] direction. Correspondingly, the quadrupole magnetic states give a threefold degenerate (Γ_{25}) mode and a doubly degenerate ($\Gamma_{12'}$) mode at $\mathbf{k}=\mathbf{0}$ which are separated into a Δ_2 and a Δ_5 band, and into a $\Delta_{1'}$ and a $\Delta_{2'}$ band along the [001] direction, respectively. Two narrow gaps open up as a result of hybridization between the extended effective-medium band and the above Δ_5 resonance bands.

In Fig. 4(b) we show the transmittance of a slab of the crystal consisting of $N_L=8$ (001) planes of spheres. The transmittance opposite the extended band exhibits the well-known Fabry-Perot oscillations due to multiple scattering between the surfaces of the slab. The period of these oscillations corresponds to $k_z a/\pi=1/8$, as expected for the given slab thickness. In the gap regions and also within regions of frequency where only nondegenerate bands exist the transmission coefficient practically vanishes.

In Fig. 5(a) we show the photonic band structure normal to the (001) surface of the crystal under consideration in more detail, over a limited frequency region about the first dipole magnetic resonance of the single sphere. Next to it, in Fig. 5(b), we show the transmittance over the same frequency region for a wave incident normally on a slab of the crystal consisting of $N_L=8$ (001) planes. Apart from the ordinary frequency bands (k_z is real) we show over the frequency gap extending from $0.70\omega_T$ to $0.78\omega_T$, the real-frequency lines with the smallest imaginary part of k_z. There are two such lines over the above region which are the analytic continuations in the complex k_z plane of the bands below and above the gap (see Fig. 6). It should be noted that the real-frequency lines in the complex k_z plane, for given $\mathbf{k}_\parallel$, satisfy some very interesting and beautiful theorems which have been studied by a number of authors in relation to the

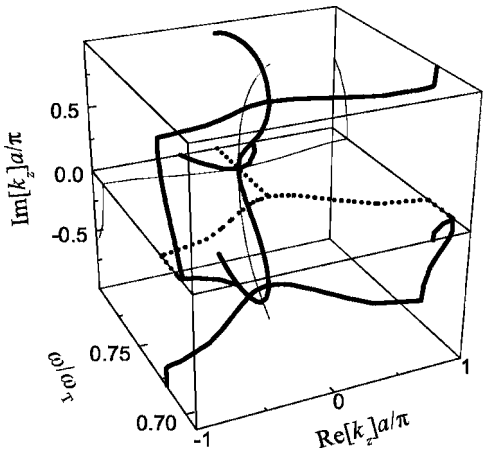

FIG. 6. The complex photonic band structure of a sc photonic crystal of nonabsorbing $LiTaO_3$ spheres ($S=0.5c/\omega_T$) in air, with $f=39.3\%$, along the [001] direction, over a limited frequency region about the first dipole magnetic resonance of the single sphere. The thick (thin) lines refer to doubly degenerate (nondegenerate) bands. The dotted lines show the projection of the complex bands on the ω-Re[k_z] plane.

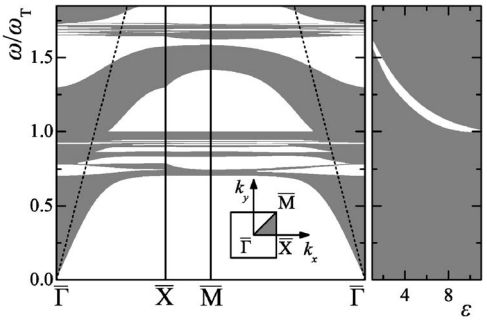

FIG. 7. Projection of the photonic band structure of a sc crystal of nonabsorbing $LiTaO_3$ spheres ($S=0.5c/\omega_T$) in air, with $f=39.3\%$, on the SBZ of the sc (001) surface, along the symmetry lines shown in the inset. The dashed line $\omega=c|\mathbf{k}_\parallel|$ shows the light cone in air. Next to this diagram we show the variation of the absolute gap (blank area) of the above crystal with the dielectric constant of the host medium.

electron band structure of crystalline solids (see, e.g., Ref. 25) and which apply also to the frequency band structure of photonic crystals. The real-frequency line of the appropriate symmetry (Δ_5 in the present case) with the smallest imaginary part over a frequency gap determines the attenuation of the wave field over this region; we obtain $\ln \mathcal{T}(\omega) = -2aN_L \,\mathrm{Im}[k_z(\omega)] + \text{const.}$, for a given value of $\mathbf{k}_\parallel$. This is demonstrated in the inset of Fig. 5(b) for a frequency within the gap. There is also an interesting observation to be made about the section of the real-frequency line extending from $0.72\omega_T$ to $0.75\omega_T$ with k_z complex and $-\pi/a < \mathrm{Re}[k_z] \leqslant \pi/a$. We remember that the band structure of Fig. 5(a) applies to the infinite crystal, and what we see in Fig. 5(b) reflects the properties of a slab of eight planes of spheres. The resonances in the transmittance of the slab suggest that at the corresponding frequencies there exist resonances of some kind in the slab, and we observe that these resonances appear within the frequency gap of the infinite crystal. These resonances (of the slab) are clearly due to resonances of the wave field localized on the individual spheres interacting very weakly between them. Of course, there can not be states of the EM field in the infinite crystal within the gap (i.e., with complex k_z). But in a slab of finite thickness such evanescent waves may exist and may lead to resonances of the EM field, with a high amplitude at the surfaces of the slab (within the spheres of the surface planes) and a much smaller amplitude in the middle of the slab (within the spheres of the middle planes). It is worth noting the fact that the resonances of the slab appear at frequencies along the real-frequency line corresponding to $\mathrm{Re}[k_z]a/\pi = \kappa/(N_L+1)$, $\kappa = 1, 2, \cdots, N_L$, where $N_L=8$ is the number of planes in the slab, as shown by the open circles in Fig. 5(a). Which implies (and we have verified this numerically) that the number of resonance dips over the gap region increases with the thickness N_L of the slab. It is as if in the slab the system remembers the narrow band (due to the weakly interacting virtual bound states of the spheres) that would be, if hybridization did not occur; in particular those states of the infinite crystal which have been removed by the hybridization "appear"on the same real-frequency line with a complex k_z (the real part of k_z is the same as before the hybridization), and manifest themselves as sharp dips in the transmittance of the slab as shown in Fig. 5(b).

In Fig. 7 we present the projection of the frequency band structure of the EM field of the photonic crystal under consideration on the symmetry lines of the SBZ of the sc (001) surface. The shaded regions extend over the frequency bands of the EM field: at any one frequency within a shaded region, for given $\mathbf{k}_\parallel$, there exists at least one propagating EM mode in the infinite crystal. The blank areas correspond to frequency gaps. We note that knowing the modes with $\mathbf{k}_\parallel$ in the shaded area ($\bar{\Gamma}\bar{X}\bar{M}$) of the SBZ and $-\pi/a < k_z \leqslant \pi/a$ is sufficient for a complete description of all the modes in the infinite crystal. The modes in the remaining of the reduced $\mathbf{k}$ space are obtained through symmetry. One clearly sees that for the given crystal one obtains an omnidirectional frequency gap, extending from $1.59\omega_T$ to $1.62\omega_T$. We verified that this is indeed so by calculating the band structure at a sufficient number of $\mathbf{k}_\parallel$ points in the SBZ. This gap results from the hybridization between the resonance band which originates from the dipole virtual bound states of the individual spheres within the polariton gap and the extended effective-medium band. The gap starts to appear at $f \approx 30\%$ and increases monotonically with f. If the dielectric constant of the host material increases, this gap is shifted to lower frequencies, as shown in the right panel of Fig. 7, because the dipole virtual bound states of the spheres within the polariton gap move to lower frequencies [$\omega_1 \approx \omega_T \sqrt{(\epsilon_0+2\epsilon)/(\epsilon_\infty+2\epsilon)}$].

V. CONCLUSION

In summary, we present a theoretical study of the optical properties of three-dimensional photonic crystals consisting of polaritonic spheres in a dielectric host medium using the layer-multiple-scattering method. Our results clarify aspects

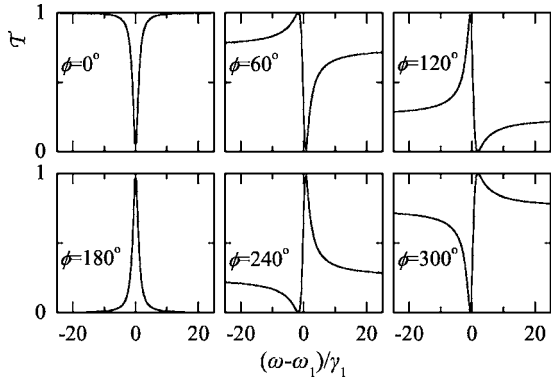

FIG. 8. Resonance structures in the transmittance of a slab according to Eq. (A7). The sequential diagrams correspond to different values of ϕ, from 0° to 300° with a step of 60°.

of the underlying physics to a degree that goes beyond existing interpretation. We analyze transmission and absorption spectra of finite slabs of these materials in conjunction with relevant complex-band-structure diagrams and develop a simple analytic model which explains the complex line shapes of the observed transmission resonances. We clarify the physical origin of the field eigenmodes and frequency gaps in these systems. Finally, we find a complete gap which increases with the fractional volume occupied by the spheres and moves down to lower frequencies by increasing the dielectric constant of the host material.

ACKNOWLEDGMENTS

This work has been supported by the research programme "Kapodistrias"of the University of Athens. G. Gantzounis was supported by the State Scholarships Foundation (I.K.Y.) of Greece.

APPENDIX

In this appendix we derive explicit expressions for the resonance structures in the transmission spectrum of EM waves through a slab of a photonic crystal. In general, the amplitudes of the incoming and outgoing waves are related through the scattering S matrix, which is unitary because of flux conservation. Let us restrict ourselves to frequencies below the first Bragg diffraction threshold, so that the scattered wave field consists of only one propagating beam. We shall further assume, for simplicity, that the slab has a (parallel) plane of mirror symmetry, so that the S matrix is symmetric. Moreover, assuming that $\mathbf{k}_\parallel$ lies in a (normal to the slab) plane of mirror symmetry so that there is no mixing between s and p waves, the S matrix takes the form

$$\mathbf{S}=\begin{pmatrix} t_s & r_s & 0 & 0 \\ r_s & t_s & 0 & 0 \\ 0 & 0 & t_p & r_p \\ 0 & 0 & r_p & t_p \end{pmatrix}, \tag{A1}$$

where $t_{s(p)}$ and $r_{s(p)}$ are the transmission and reflection amplitudes, respectively, for $s(p)$-polarized waves. It is straightforward to show that the eigenvalues of the S matrix are t_s+r_s, t_s-r_s, t_p+r_p, t_p-r_p, and, since $\mathbf{S}$ is unitary, these can be written as

$$t_s+r_s=\exp(2i\delta_{s+}),\ t_s-r_s=\exp(2i\delta_{s-}),$$

$$t_p+r_p=\exp(2i\delta_{p+}),\ t_p-r_p=\exp(2i\delta_{p-}), \tag{A2}$$

where δ_{s+}, δ_{s-}, δ_{p+}, δ_{p-}, the so-called scattering phase shifts, are real functions of frequency. Using Eqs. (A2), the transmittance of the slab can be expressed in terms of the scattering phase shifts as follows:

$$\mathcal{T}\equiv|t_{s(p)}|^2=\frac{1}{2}\{1+\cos[2(\delta_{s(p)+}-\delta_{s(p)-})]\}, \tag{A3}$$

for a $s(p)$-polarized incident wave. On the other hand, the change in the number of states up to a given frequency, induced by the slab, is given by[26]

$$\Delta N=\frac{1}{2\pi}\,\mathrm{Im}\ln\det\mathbf{S}$$

$$=\frac{1}{\pi}(\delta_{s+}+\delta_{s-}+\delta_{p+}+\delta_{p-}). \tag{A4}$$

Let us now consider the analytic continuation of the eigenvalues of the S matrix in the complex frequency plane. The causality condition implies that these functions are analytic in the upper half-plane but they may have poles in the lower half-plane at $\omega_i-i\gamma_i$, $\gamma_i\geqslant 0$, which correspond to zeros at $\omega_i+i\gamma_i$. Among all possible solutions, those with $\gamma_i/\omega_i\ll 1$ are of particular physical interest. Assuming the existence of such a simple pole at $\omega_1-i\gamma_1$, separated from the other poles, in the vicinity of this point, on the real axis, the corresponding eigenvalue has the form $\exp(2i\alpha)(\omega-\omega_1-i\gamma_1)/(\omega-\omega_1+i\gamma_1)$. We assume that α as well as the phase shifts associated with the other eigenvalues of the S matrix do not vary considerably with frequency in the vicinity of the pole, where the frequency dependence is dominated by the resonant part, $\delta_1(\omega)$, of the relevant phase shift, where

$$\cos[2\delta_1(\omega)]=\frac{(\omega-\omega_1)^2-\gamma_1^2}{(\omega-\omega_1)^2+\gamma_1^2},$$

$$\sin[2\delta_1(\omega)]=\frac{-2\gamma_1(\omega-\omega_1)}{(\omega-\omega_1)^2+\gamma_1^2}. \tag{A5}$$

The change of the density of states in the vicinity of the pole is obtained from Eqs. (A4) and (A5)

$$\Delta n(\omega)=\frac{d\Delta N(\omega)}{d\omega}\approx\frac{1}{\pi}\frac{\gamma_1}{(\omega-\omega_1)^2+\gamma_1^2}, \tag{A6}$$

and has the form of a Lorentzian resonance centered at ω_1. Its width is determined by γ_1 and its integral equals unity. Since $\gamma_1/\omega_1\ll 1$, this resonance mode resembles a bound state: it has a long (though not infinite) lifetime and the field intensity associated with it is mostly concentrated within the slab (though it leaks, to some minor degree, in the host region). Such states are referred to as virtual bound states.

In turn, the resonant transmittance of the slab near the frequency region of the virtual bound state is obtained from Eqs. (A3) and (A5)

$$\mathcal{T} \approx \frac{1}{2}\left[1 + \frac{(\omega-\omega_1)^2-\gamma_1^2}{(\omega-\omega_1)^2+\gamma_1^2}\cos\phi - \frac{2\gamma_1(\omega-\omega_1)}{(\omega-\omega_1)^2+\gamma_1^2}\sin\phi\right], \tag{A7}$$

where ϕ is a phase which contains the contribution of the non-resonant phase shifts and can be considered as constant within a short range of frequencies about the resonance. Equation (A7) tells us that, depending on the value of ϕ, a virtual bound state can induce different resonance structures in the transmission spectrum, as shown in Fig. 8. The generalization of the formulas derived in this appendix to cases where more than one resonances contribute within a given region of frequency is straightforward.

[1] J. D. Joannopoulos, R. D. Meade, and J. N. Winn, *Photonic Crystals: Molding the Flow of Light* (Princeton University Press, Princeton, NJ, 1995).

[2] K. Sakoda, *Optical Properties of Photonic Crystals* (Springer-Verlag, Berlin, 2001).

[3] M. M. Sigalas, C. M. Soukoulis, C. T. Chan, and K. M. Ho, Phys. Rev. B **49**, 11080 (1994).

[4] W. Zhang, A. Hu, X. Lei, N. Xu, and N. Ming, Phys. Rev. B **54**, 10280 (1996).

[5] W. Zhang, A. Hu, and N. Ming, J. Phys.: Condens. Matter **9**, 541 (1997).

[6] V. Kuzmiak, A. A. Maradudin, and A. R. McGurn, Phys. Rev. B **55**, 4298 (1997).

[7] W. Zhang, Z. Wang, A. Hu, and N. Ming, J. Phys.: Condens. Matter **12**, 5307 (2000).

[8] R. Moussa, L. Salomon, F. de Fornel, J. P. Dufour, and H. Aourag, Infrared Phys. Technol. **44**, 27 (2003).

[9] K. C. Huang, P. Bienstman, J. D. Joannopoulos, K. A. Nelson, and S. Fan, Phys. Rev. Lett. **90**, 196402 (2003).

[10] K. C. Huang, P. Bienstman, J. D. Joannopoulos, K. A. Nelson, and S. Fan, Phys. Rev. B **68**, 075209 (2003).

[11] A. Rung and C. G. Ribbing, Phys. Rev. Lett. **92**, 123901 (2004).

[12] K. C. Huang, E. Lidorikis, X. Jiang, J. D. Joannopoulos, K. A. Nelson, P. Bienstman, and S. Fan, Phys. Rev. B **69**, 195111 (2004).

[13] K. C. Huang, M. L. Povinelli, and J. D. Joannopoulos, Appl. Phys. Lett. **85**, 543 (2004).

[14] V. Yannopapas and A. Moroz, J. Phys.: Condens. Matter **17**, 3717 (2005).

[15] N. Stefanou, V. Karathanos, and A. Modinos, J. Phys.: Condens. Matter **4**, 7389 (1992).

[16] N. Stefanou, V. Yannopapas, and A. Modinos, Comput. Phys. Commun. **113**, 49 (1998).

[17] N. Stefanou, V. Yannopapas, and A. Modinos, Comput. Phys. Commun. **132**, 189 (2000).

[18] C. Kittel, *Introduction to Solid State Physics* (Wiley, New York, 1976).

[19] M. Schall, H. Helm, and S. R. Keiding, Int. J. Infrared Millim. Waves **20**, 595 (1999).

[20] G. Gantzounis, N. Stefanou, and V. Yannopapas, J. Phys.: Condens. Matter **17**, 1791 (2005).

[21] J. F. Cornwell, *Group Theory and Electronic Energy Bands in Solids* (North-Holland, Amsterdam, 1969).

[22] K. Ohtaka and Y. Tanabe, J. Phys. Soc. Jpn. **65**, 2670 (1996).

[23] R. Ruppin, Opt. Commun. **182**, 273 (2000).

[24] V. Karathanos, J. Mod. Opt. **45**, 1751 (1998).

[25] V. Heine, Proc. Phys. Soc. London **81**, 300 (1963).

[26] K. Ohtaka, Y. Suda, S. Nagano, T. Ueta, A. Imada, T. Koda, J. S. Bae, K. Mizuno, S. Yano, and Y. Segawa, Phys. Rev. B **61**, 5267 (2000).